





The FlgN chaperone activates the Na⁺-driven engine of the *Salmonella* flagellar protein export apparatus

Tohru Minamino ^{1✉}, Miki Kinoshita ¹, Yusuke V. Morimoto ^{2,3} & Keiichi Namba ^{1,4,5}

The bacterial flagellar protein export machinery consists of a transmembrane export gate complex and a cytoplasmic ATPase complex. The gate complex has two intrinsic and distinct H⁺-driven and Na⁺-driven engines to drive the export of flagellar structural proteins. *Salmonella* wild-type cells preferentially use the H⁺-driven engine under a variety of environmental conditions. To address how the Na⁺-driven engine is activated, we analyzed the *fliJ*($\Delta 13-24$) *fliH*($\Delta 96-97$) mutant and found that the interaction of the FlgN chaperone with FlhA activates the Na⁺-driven engine when the ATPase complex becomes non-functional. A similar activation can be observed with either of two single-residue substitutions in FlhA. Thus, it is likely that the FlgN-FlhA interaction generates a conformational change in FlhA that allows it to function as a Na⁺ channel. We propose that this type of activation would be useful for flagellar construction under conditions in which the proton motive force is severely restricted.

¹Graduate School of Frontier Biosciences, Osaka University, Osaka, Japan. ²Department of Physics and Information Technology, Faculty of Computer Science and Systems Engineering, Kyushu Institute of Technology, Fukuoka, Japan. ³Japan Science and Technology Agency, PRESTO, Saitama, Japan. ⁴RIKEN SPring-8 Center and Center for Biosystems Dynamics Research, Osaka, Japan. ⁵JEOL YOKOGUSHI Research Alliance Laboratories, Osaka University, Osaka, Japan. ✉email: tohru@fbs.osaka-u.ac.jp

The bacterial flagellum is a macromolecular protein complex responsible for rapid and efficient movement of bacterial cells towards more suitable environments. The flagellum is composed of the basal body, which acts as a rotary motor, the hook, which serves as a universal joint, and the filament, which forms a helical propeller^{1,2}. To construct the flagellum on the cell surface, a specialized protein export machinery located at the flagellar base transports flagellar structural subunits from the cytoplasm to the distal end of the growing flagellar structure. The flagellar export machinery is composed of a transmembrane export gate complex powered by a proton motive force (PMF) across the cytoplasmic membrane and a cytoplasmic ATPase ring complex^{3,4}. This export machinery is structurally and functionally similar to virulence-related type III secretion systems of pathogenic bacteria, which directly inject virulence effector proteins into eukaryotic host cells⁵.

The transmembrane export gate complex is located inside the basal body MS ring and acts as a proton/protein antiporter to drive H⁺-coupled protein translocation across the cytoplasmic membrane^{3,4}. FliP, FliQ, and FliR form a polypeptide channel complex for the translocation of export substrates across the cytoplasmic membrane^{6,7}. FlhB associates with the FliP/FliQ/FliR complex and is postulated to coordinate opening of the polypeptide channel⁸. FlhA associates not only with the FliP/FliQ/FliR complex but also with the MS ring⁹. Because FlhA promotes the transit of both H⁺ and Na⁺ across the cytoplasmic membrane, it seems to act as the export engine of the export gate complex^{10,11}. The C-terminal cytoplasmic domains of FlhA (FlhA_C) and FlhB (FlhB_C) project into the central cavity of the basal body C ring and form a docking platform for the cytoplasmic ATPase complex (FliH, FliI, FliJ), flagellar chaperones (FlgN, FliS, FliT) and export substrates^{12,13}. This docking platform coordinates the order of flagellar protein export with assembly in a highly organized and well-controlled manner¹⁴.

FliH, FliI, and FliJ form the cytoplasmic ATPase ring complex at the flagellar base¹⁵. This structure is not essential for flagellar protein export in *Salmonella enterica* serovar Typhimurium (hereafter referred to as *Salmonella*)^{16–18}, but it ensures robust and efficient coupling of energy to flagellar protein export^{19,20}. The FliI ATPase

hydrolyses ATP and activates the export gate complex through an interaction between FlhA_C and FliJ, which is located at the center of the FliI hexamer ring, thereby allowing the transmembrane export gate complex to become active in coupling influx of H⁺ through the FlhA ion channel with the translocation of export substrates through the FliP/FliQ/FliR polypeptide channel^{21–23}.

The export gate complex can also use a sodium motive force (SMF) across the cytoplasmic membrane to drive Na⁺-coupled protein export when the cytoplasmic ATPase ring complex is absent or nonfunctional¹⁰. Because the FlhA ion channel conducts both H⁺ and Na⁺, it is plausible that the ATPase complex may switch the ion channel properties of FlhA from a dual ion mode to a highly efficient H⁺ channel through an interaction between FlhA_C and FliJ¹⁰. However, it remains unknown how this might happen.

In planktonic *Salmonella* wild-type cells, the transmembrane export gate complex preferentially uses the PMF to transport flagellar structural subunits to the cell exterior under a variety of environmental conditions^{16–18,21}. However, when the cytoplasmic ATPase ring complex becomes nonfunctional, as during biofilm formation²⁴, the export gate preferentially uses the SMF over a wide range of external pH¹⁰. A subpopulation of planktonic cells can rapidly move in the biofilm structure by rotating flagella to keep cells in the biofilm alive and healthy²⁵. The second messenger molecule 3'-5' cyclic diguanylate monophosphate, which induces biofilm formation, not only inhibits the transcription of flagellar genes but also binds to the FliI ATPase to suppress flagellar assembly of the cells in the biofilm²⁴. The total PMF seems to be quite low in the cells living in the biofilm because the membrane voltage is quite small²⁶. These observations suggest that the flagellar protein export apparatus would evolve to retain the Na⁺-driven export engine so that flagellated cells could arise in biofilms.

To clarify how the Na⁺-driven export engine is activated, we analyzed the export properties of the *Salmonella* MM104H-3 [*fliJ*(Δ13–24) *fliH*(Δ96–97)] strain (hereafter referred to as J_(Δ13–24) H*, Table 1), in which the extragenic *fliH* suppressor

Table 1 Summary for important properties of *Salmonella* strains with respect to motility, flagellar protein export and flagellar assembly.

Strains	Abbreviated name	NaCl (mM)	Motility	Flagellar protein export		Flagellar assembly	
				FlgD secretion	FliC secretion	HBB ^a	Filament
SJW1103 (Wild-type)	WT	0	++++	+++	+++	N.A. ^b	+++
MM104-3 [<i>fliJ</i> (Δ13–24) <i>fliH</i> *]	J _(Δ13–24) H	100	++++	+++	+++	+	++++
		0	+	+++	+++	N.A.	++
MMHI1017(Δ <i>fliH</i> <i>fliB</i> *)	ΔHI B*	100	++	++++	++++	+	+++
		0	+/-	+/-	-	N.A.	N.A.
MMHIJ1017 (Δ <i>fliHIJ</i> <i>fliB</i> *)	ΔHIJ B*	100	++	+++	++	N.A.	++
		0	+/-	-	-	N.A.	N.A.
MMHIJ1017-2 [Δ <i>fliHIJ</i> <i>fliB</i> * <i>fliA</i> (D456V)]	ΔHIJ B* A1*	100	+	+	+	N.A.	+
		100	N.A.	+++	+++	N.A.	++
MMHIJ1017 [Δ <i>fliHIJ</i> <i>fliB</i> * <i>fliA</i> (T490M)]	ΔHIJ B* A2*	100	+	+++	+++	N.A.	++
		100	+	+++	+++++	+	+/-
MM9001(Δ <i>flgN</i>)	ΔN	100	-	-	-	-	-
MM9003 [<i>fliJ</i> (Δ13–24) <i>fliH</i> * Δ <i>flgN</i>]	J _(Δ13–24) H ΔN	100	+	++++	++++	N.A.	N.A.
MM9003-2 [<i>fliJ</i> (Δ13–24) <i>fliH</i> * Δ <i>flgN</i> <i>fliA</i> (D456V)]	J _(Δ13–24) H ΔN A1*	100	+	++++	++++	N.A.	N.A.
MM9003-3 [<i>fliJ</i> (Δ13–24) <i>fliH</i> * Δ <i>flgN</i> <i>fliA</i> (T490M)]	J _(Δ13–24) H ΔN A2*	100	+	++++	++++	N.A.	N.A.
MM9002 (Δ <i>fliHI</i> <i>fliB</i> * Δ <i>flgN</i>)	ΔHI B* ΔN	100	-	-	-	N.A.	-
MM9004 (Δ <i>fliHIJ</i> <i>fliB</i> * Δ <i>flgN</i>)	ΔHIJ B* ΔN	100	-	-	-	N.A.	-
MM9004-2 [Δ <i>fliHIJ</i> <i>fliB</i> * Δ <i>flgN</i> <i>fliA</i> (D456V)]	ΔHIJ B* ΔN A1*	100	N.A.	+++	+++	N.A.	+/-
MM9004-3 [Δ <i>fliHIJ</i> <i>fliB</i> * Δ <i>flgN</i> <i>fliA</i> (T490M)]	ΔHIJ B* ΔN A2*	100	N.A.	+++	+++	N.A.	+/-

^aHBB hook-basal body.

^bN.A. not analyzed.

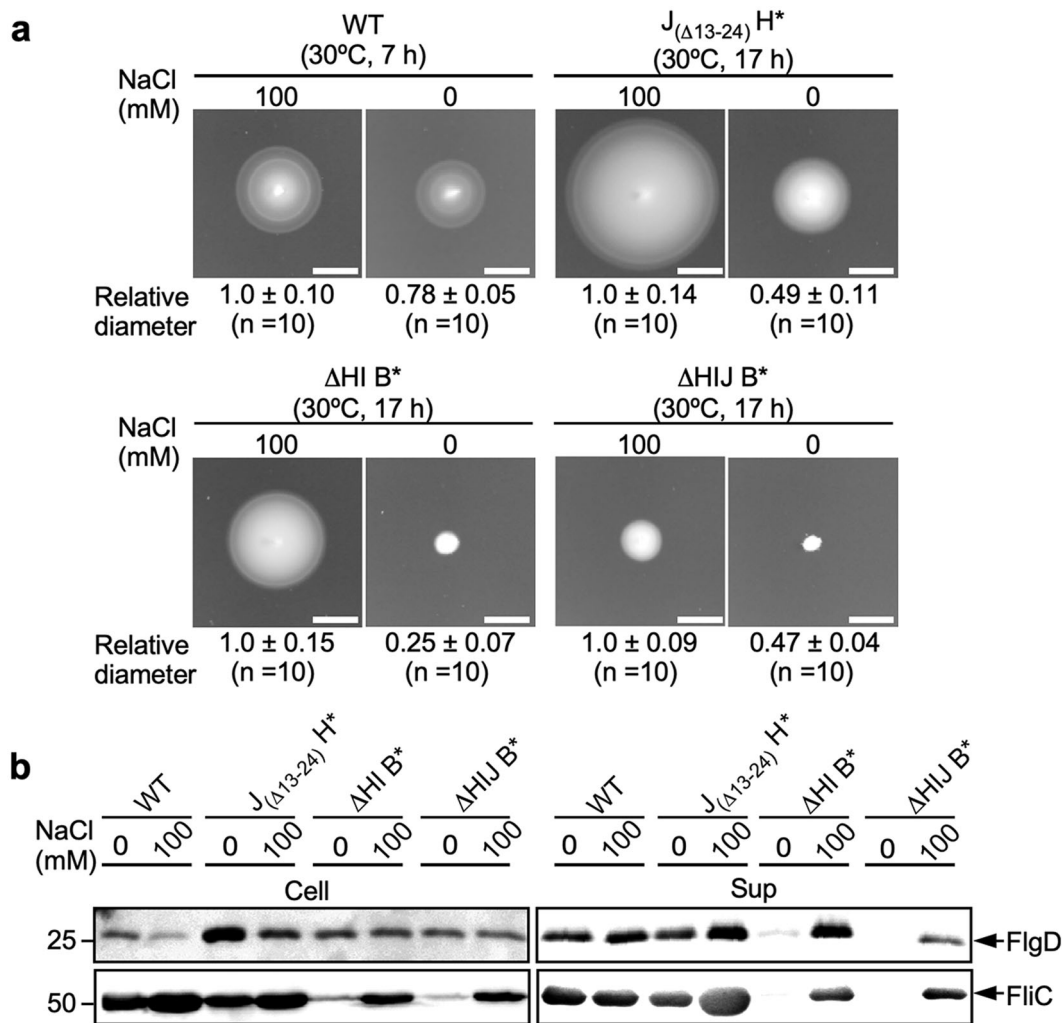


Fig. 1 Effect of Na^+ ions on flagellar protein export. **a** Motility of SJW1103 (wild-type, indicated as WT), MM104H-3 [$fliJ(\Delta 13-24) fliH(\Delta 96-97)$, indicated as $J_{(\Delta 13-24)} H^*$], MMH10117 [$\Delta fliH-fliI flhB(P28T)$, indicated as $\Delta HI B^*$] and MMH10117 [$\Delta fliH-fliI-fliJ flhB(P28T)$, indicated as $\Delta HIJ B^*$] in 0.35% soft agar plates in the absence and presence of 100 mM NaCl. The diameter of the motility ring of 10 colonies of each strain was measured in the presence and absence of 100 mM NaCl. The average diameter of the motility ring of each strain grown in the presence of 100 mM NaCl was set to 1.0, and then relative diameter of the motility ring of cells grown in the absence of NaCl was calculated (mean \pm SD, $n = 10$). Scar bar, 1.0 cm. **b** Effect of Na^+ on flagellar protein export at external pH 7.5. Immunoblotting, using polyclonal anti-FlgD or anti-FliC antibody, of whole-cell proteins (Cell) and culture supernatant fractions (Sup) prepared from the above strains grown exponentially at 30 °C in T-broth (pH 7.5) with or without 100 mM NaCl. The regions of interest were cropped from original immunoblots shown in Supplementary Fig. 10.

mutation partially rescues the interaction of FliJ($\Delta 13-24$) with FlhA_C, thereby restoring flagellar formation in the presence of the $fliJ(\Delta 13-24)$ mutation²¹. We show that the $J_{(\Delta 13-24)} H^*$ cells use the SMF to produce flagella and that an interaction of FlhA_C with FlgN is essential for this Na^+ -coupled protein export.

Results

Effect of the SMF on flagellar protein export by the $J_{(\Delta 13-24)} H^*$ strain. To clarify whether an altered interaction of FliJ with FlhA_C induces opening of a Na^+ channel in FlhA, we analyzed the effect of the SMF on flagellar formation by the $J_{(\Delta 13-24)} H^*$ strain, in which FliJ has a decreased affinity for FlhA_C²¹. We set the external pH at 7.5 to diminish the chemical potential gradient of H^+ ²⁷ and confirmed that was the case by using a pH indicator protein, pHluorin(M153R)^{28,29} to show that the intracellular pH of *Salmonella* cells was 7.41 ± 0.05 . The results for all strains we used in this study are qualitatively summarized in Table 1.

Motility of the $J_{(\Delta 13-24)} H^*$ strain was better in the presence of 100 mM NaCl than in its absence (Fig. 1a and Supplementary Fig. 1). The amount of FlgD and FliC secreted by these cells was also higher in the presence of 100 mM NaCl than in its absence (Fig. 1b). Because the growth rate of *Salmonella* cells is slower under no-salt conditions compared to in the presence of 100 mM NaCl or 100 mM KCl (Supplementary Fig. 2), we also analyzed the motility of the $J_{(\Delta 13-24)} H^*$ cells in the presence of 100 mM KCl. These cells were less motile in the presence of 100 mM KCl than in the presence of 100 mM NaCl (Supplementary Fig. 3a). Also, unlike NaCl, KCl did not enhance the secretion level of FliC (Supplementary Fig. 3b). These results demonstrate that Na^+ facilitates protein export by the $J_{(\Delta 13-24)} H^*$ cells, whereas neither motility nor flagellar protein export by wild-type cells showed any Na^+ dependence (Fig. 1 and Supplementary Fig. 3), in agreement with a previous report¹⁰.

To quantify the efficiency of flagellar assembly, we labelled the filaments with a fluorescent dye (Fig. 2a) and measured the

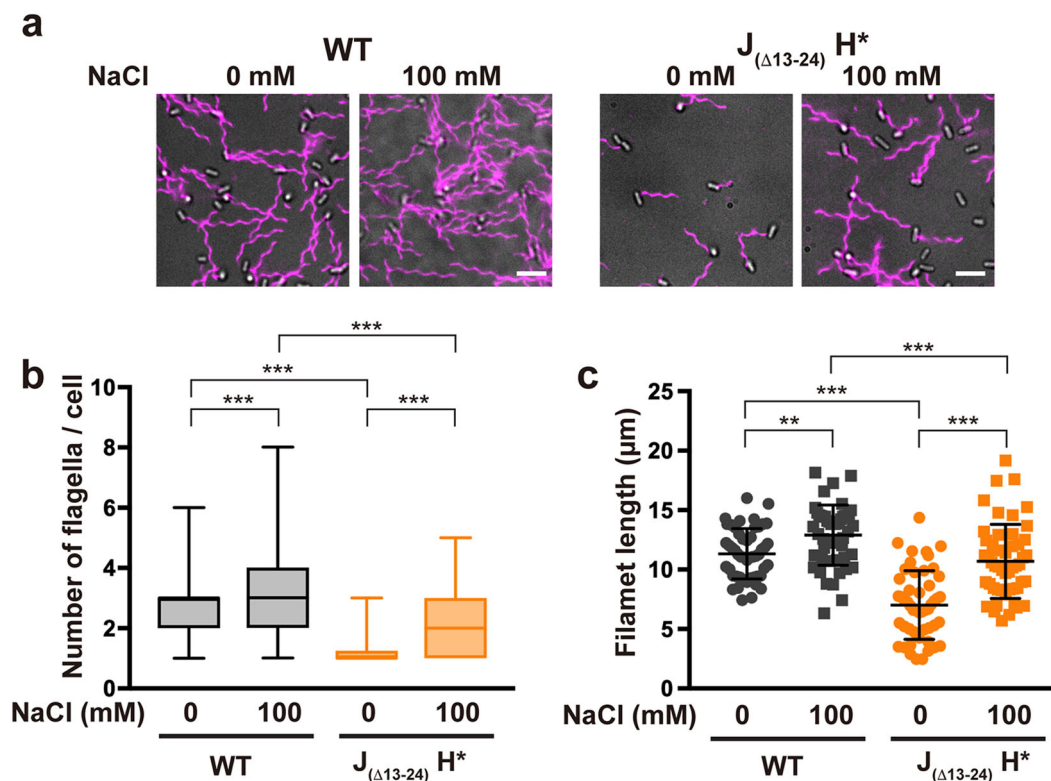


Fig. 2 Measurements of the number and length of flagellar filaments produced by the $J_{(\Delta 13-24)} H^*$ strain. **a** Fluorescent images of the SJW1103 (WT) and MM104H-3 ($J_{(\Delta 13-24)} H^*$) cells. The cells were grown in T-broth (pH 7.5) with or without 100 mM NaCl until the cells reached the stationary phase, and then flagellar filaments were labelled with a fluorescent dye, Alexa Fluor 594. The fluorescence images of the filaments labelled with Alexa Fluor 594 (magenta) were merged with the bright field images of the cell bodies. Scale bar, 5.0 μm . **b** Average number of flagellar filaments. Box plots show the number of the flagellar filaments in the WT and $J_{(\Delta 13-24)} H^*$ cells. Lower and upper box boundaries are 25th and 75th percentiles, respectively. The line in the middle of the box is median. Lower and upper error lines are the smallest and largest values, respectively. More than 110 cells were counted. **c** Scatter plots of flagellar filament length. Filament length is the average of 50 filaments, and vertical lines are standard deviations. Comparisons between datasets were performed using a two-tailed Student's *t*-test. A *P*-value of <0.05 was considered to be statistically significant difference. ***P* < 0.01 ; ****P* < 0.001 . (Also see Supplementary Table 1).

number and length of the filaments (Supplementary Table 1). Wild-type cells produced an average of 2.7 ± 1.1 filaments per cell (mean \pm SD, $n = 152$) in the absence of NaCl and 3.3 ± 1.5 filaments per cell ($n = 153$) in the presence of 100 mM NaCl (Fig. 2b). The average filament length was $11.3 \pm 2.1 \mu\text{m}$ ($n = 50$) in the absence of NaCl and $12.9 \pm 2.5 \mu\text{m}$ ($n = 50$) in the presence of 100 mM NaCl (Fig. 2c). Because the transcription levels of flagellar genes were not increased by adding 100 mM NaCl¹⁰, we suggest that the wild-type protein export apparatus may also utilize the SMF to some extent. In the absence of NaCl, 38.5% of the $J_{(\Delta 13-24)} H^*$ cells had no visible filaments. The remaining population produced an average of 1.3 ± 0.5 filaments per cell ($n = 118$) (Fig. 2b). The average filament length was $7.0 \pm 2.9 \mu\text{m}$ ($n = 50$), which is about 1.6-fold shorter than the length of the wild-type filaments in the absence of NaCl (Fig. 2c), indicating that the growth rate of filaments in these cells is slower than in the wild-type. In contrast, 87.3% of the $J_{(\Delta 13-24)} H^*$ cells produced the filaments in the presence of 100 mM NaCl, with an average number of 2.0 ± 1.0 per cell ($n = 145$) (Fig. 2b). The average filament length was $10.7 \pm 3.1 \mu\text{m}$ ($n = 50$), which is about 1.5-fold longer than the filament length of cells grown without NaCl (Fig. 2c). These results suggest that the transmembrane export gate complex of this strain uses the SMF in addition to the PMF to transport flagellar structural proteins during flagellar assembly. Based on these results, we propose that an altered interaction between FliJ and FlhA_C activates a Na⁺-driven export engine to promote Na⁺-coupled flagellar protein export.

Effect of FlgN on flagellar protein export by $J_{(\Delta 13-24)} H^*$ cells.

The *Salmonella* MMH10117 [$\Delta fliH-fliI flhB(P28T)$] strain (hereafter referred to as $\Delta HI B^*$, Table 1) is a pseudorevertant isolated from a mutant with a deletion of the two genes that form the cytoplasmic ATPase complex¹⁶. The $\Delta HI B^*$ cells also preferentially use the SMF rather than the PMF to produce flagella and support some motility (Fig. 1a)¹⁰. Under no-salt conditions, FliC is not expressed in the $\Delta HI B^*$ strain (Fig. 1b) because FlgM, the transcription repressor of class 3 flagellar proteins such as FliC until hook assembly is complete^{30,31}, is also not secreted out of the cytoplasm (Supplementary Fig. 4). In agreement with a previous report¹⁰, addition of 100 mM KCl did not enhance motility or flagellar protein export by the $\Delta HI B^*$ cells (Supplementary Fig. 3). It has been shown that a nonfunctional variant of FliJ, GST-FliJ, binds to FlhA and inhibits flagellar protein export by the $\Delta HI B^*$ cells³². Therefore, to identify the flagellar protein required for activation of the Na⁺-driven export engine, GST-FliJ was overexpressed in $\Delta HI B^*$ cells, and whole-cell lysates were subjected to GST affinity chromatography. In addition to FlhA, FlgN also co-purified with GST-FliJ, but not with GST alone (Supplementary Fig. 5). FlgN is a flagellar export chaperone specific for two hook-filament junction proteins, FlgK and FlgL³³. The FlgN chaperone protects these two proteins from proteolysis in the cytoplasm³⁴ and also facilitates the docking of FlgK and FlgL to FlhA_C to expedite rapid and efficient export of these proteins³⁵⁻³⁷. Unlike the FliS and FliT chaperones, which

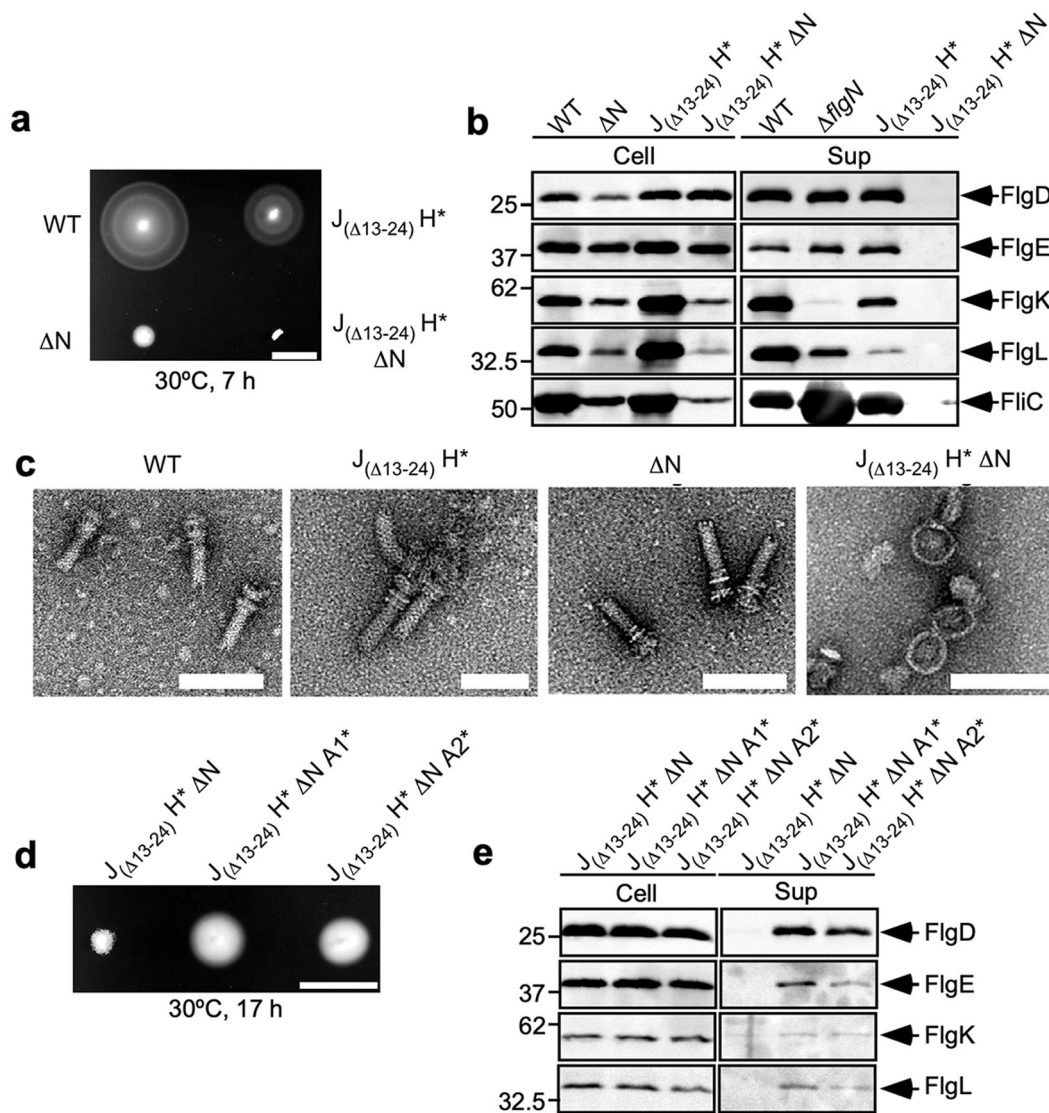


Fig. 3 Effect of FlgN deletion on flagellar protein export by *fliJ*($\Delta 13-24$) *fliH** cells. **a** Motility of SJW1103 (WT), MM104H-3 (*J*($\Delta 13-24$) *H**), MM9001 (ΔN) and MM9003 (*J*($\Delta 13-24$) *H** ΔN) in 0.35% soft agar plates containing 100 mM NaCl. Scale bar, 1.0 cm. **b** Immunoblotting, using polyclonal anti-FlgD (1st row), anti-FlgE (2nd row), anti-FlgK (3rd row), anti-FlgL (4th row) or anti-FliC (5th row) antibody, of whole-cell proteins (Cell) and culture supernatant fractions (Sup) prepared from the above strains. The regions of interest were cropped from original immunoblots shown in Supplementary Fig. 11a. **c** Electron micrographs of hook-basal bodies isolated from the above stains. Scale bar, 100 nm. **d** Motility of MM9003, MM9003-2 (*J*($\Delta 13-24$) *H** ΔN A1*) and MM9003-3 (*J*($\Delta 13-24$) *H** ΔN A2*) in 0.35% soft agar plates containing 100 mM NaCl. Scale bar, 1.0 cm. **e** Immunoblotting, using polyclonal anti-FlgD (1st row), anti-FlgE (2nd row), anti-FlgK (3rd row), or anti-FlgL (4th row) antibody, of whole-cell proteins (Cell) and culture supernatant fractions (Sup) prepared from the above strains. The regions of interest were cropped from original immunoblots shown in Supplementary Fig. 11b.

require their cognate export substrates, FliC and FliD, respectively, to bind to FlhA_C, FlgN binds to FlhA_C with nanomolar affinity even in the absence of FlgK and FlgL³⁶. This property of FlgN raises the question of whether its interaction with FlhA_C activates the Na⁺-driven export engine.

To answer this question, we introduced a *ΔflgN::tetRA* allele into the wild-type and *J*($\Delta 13-24$) *H** strains by P22-mediated transduction to produce the *ΔflgN* and *J*($\Delta 13-24$) *H** *ΔflgN* strains (hereafter referred to as ΔN and *J*($\Delta 13-24$) *H** ΔN , respectively, Table 1) and analyzed motility of these two transductants in soft agar. About 35.2% of the ΔN cells produced a single flagellar filament (Supplementary Fig. 6a), and this level of flagellar synthesis was sufficient to generate a small motility ring on soft agar plates (Fig. 3a). In contrast, the *J*($\Delta 13-24$) *H** ΔN cells were completely nonmotile (Fig. 3a), and no filaments were seen on these cells (Supplementary Fig. 6a).

To discover why the *J*($\Delta 13-24$) *H** ΔN cells do not produce flagellar filaments, we next analyzed the impact of *ΔflgN::tetRA* on flagellar protein export. The loss of FlgN considerably reduced the levels of FlgK and FlgL secreted by wild-type cells but had little effect on secretion of the hook-capping protein, FlgD or the hook protein, FlgE (Fig. 3b). The ΔN cells produced visible hook-basal bodies (HBBs) (Fig. 3c), in agreement with a previous report³⁸. In contrast, the presence of *ΔflgN::tetRA* inhibited the secretion of FlgD and FlgE by the *J*($\Delta 13-24$) *H** cells (Fig. 3b). Whereas the *J*($\Delta 13-24$) *H** cells produced HBBs, the *J*($\Delta 13-24$) *H** cells containing *ΔflgN::tetRA* produced only the MS-C ring structures (Fig. 3c). Also, the intracellular levels of FliC, FlgK and FlgL were much lower in the absence of FlgN than in its presence in the *J*($\Delta 13-24$) *H** mutant background (Fig. 3b), suggesting that FlgN is also required for FlgM secretion. When FlgN was expressed from a pTrc99A based plasmid in the *J*($\Delta 13-24$) *H** ΔN cells, the motility

was restored to a level comparable to that of the $J_{(\Delta 13-24)}$ H* strain (Supplementary Fig. 6b). These results indicate that FlgN becomes essential for the export of all flagellar structural proteins by the $J_{(\Delta 13-24)}$ H* cells.

The Δ HI B* and MMHIJ0117 [Δ *fliH-fliI-fliJ flhB(P28T)*] (hereafter referred to as Δ HIJ B*, Table 1) cells showed a clear Na⁺ dependence on flagellar protein export (Fig. 1 and Supplementary Fig. 3). To confirm our observations described above, we also introduced the Δ *flgN::tetRA* allele into these two strains and found that a loss of FlgN results in a completely nonmotile phenotype (Fig. 4a and Supplementary Fig. 6b). Also, neither FlgD, FliC nor FlgM were seen in the culture supernatants of these two strains containing Δ *flgN::tetRA* (Fig. 4b and Supplementary Figs 7 and 8). Therefore, we conclude that FlgN is essential for Na⁺-coupled protein export by the transmembrane export gate complex when the functional cytoplasmic ATPase complex is absent.

Pseudorevertants of the $J_{(\Delta 13-24)}$ H* Δ N cells. The *flhA(D456V)* or *flhA(T490M)* mutation partially restores motility to the Δ HI B* strain lacking FlgN³⁵ (Supplementary Fig. 7). Therefore, we introduced these alleles into the $J_{(\Delta 13-24)}$ H* Δ N cells by P22-mediated transduction to see whether motility was rescued. As expected, either of these *flhA* mutations improved motility and flagellar protein export (Fig. 3d and e), indicating that these *flhA* mutations can also activate the Na⁺-driven export engine in the absence of FlgN. Therefore, we suggest that these single-residue substitutions in FlhA_C allow FlhA_C to adopt a conformation mimicking a FlgN-bound state of FlhA_C, thereby allowing the export gate complex to utilize the SMF to transport flagellar structural subunits to the cell exterior even in the absence of FlgN.

Effect of deletion of FliJ residues 13–24 on the interactions of FlgN and FlhA_C. The interaction of FliJ with the linker region of FlhA_C (FlhA_L) is required for activation of the transmembrane export gate complex, and FliH and FliI are required for efficient interaction between FliJ and FlhA_L^{21,32}. In addition to binding with high affinity to FlhA_C, FlgN binds to FliJ with a K_D of 22 μ M³⁹. Thus, FlgN may be important in the docking of FliJ to FlhA_C, especially when the functions of FliH and FliI are compromised. Therefore, we first investigated whether the *fliJ* (Δ 13–24) deletion mutation affects the interaction of FliJ with FlgN. FlgN co-purified with GST-FliJ(Δ 13–24) (Fig. 5a), indicating that the deletion does not abolish interaction with FlgN. To assess the strength of the FliJ-FlgN interaction, we examined binding of FlgN to immobilized GST-FliJ or GST-FliJ(Δ 13–24) by surface plasmon resonance (SPR). Steady-state analysis of the SPR data with a 1 to 1 binding model indicated that the K_D values for the FliJ-FlgN and FliJ(Δ 13–24)-FlgN interactions were $27.4 \pm 13.0 \mu$ M and $7.74 \pm 0.12 \mu$ M, respectively (Fig. 5b). Thus, the deletion actually increases the binding affinity by about 3.5-fold.

We next investigated whether FlgN participates in the interaction of FliJ(Δ 13–24) with FlhA_C. The amount of FlhA_C that co-purified with GST-FliJ(Δ 13–24) was much lower than that with GST-FliJ (Fig. 5c and d, upper panels), in agreement with a previous report²¹. FlgN did not improve the interaction of FliJ (Δ 13–24) with FlhA_C (lower panels). These results suggest that a direct interaction between FlgN and FlhA_C turns on Na⁺-coupled protein export independently of FliJ when the FliJ-FlhA_C interaction is compromised.

Effect of the *flhA(D456V)* and *flhA(T490M)* mutations on Na⁺-coupled protein export by cells lacking FliH, FliI, and FliJ. FliJ is apparently more important for Na⁺-coupled flagellar protein

export than FliH and FliI²¹ because the protein export activity of the Δ HIJ B* strain is much lower than that of the Δ HI B* strain (Fig. 1 and Supplementary Fig. 1). To confirm this, we first analyzed the number and length of flagellar filaments produced by the Δ HI B* and Δ HIJ B* cells (Fig. 4a and Supplementary Table 2). About 78.2% of the Δ HI B* cells produced the filaments with an average of 1.6 ± 0.7 filaments per cell ($n = 266$) and an average length of $7.8 \pm 2.5 \mu$ m ($n = 50$) (Fig. 4c, d). In contrast, only 13.5% of the Δ HIJ B* cells produced the filaments with an average of 1.1 ± 0.2 filaments per cell ($n = 57$) and an average length of $5.1 \pm 2.2 \mu$ m ($n = 50$) (Fig. 4c, d). Therefore, we conclude that FliJ is required for efficient activation of the export gate complex even in the absence of FliH and FliI.

Since FliJ is not critical for activation of the Na⁺-driven export engine, we hypothesized that the interaction of FliJ with FlhA_C may be required for efficient opening of the polypeptide channel for the substrate entry into the channel. Because it has been shown that the *flhA(D456V)* or *flhA(T490M)* mutation significantly increases the probability of entry of export substrates such as FlgD and FlgE into the polypeptide channel in the Δ HI B* cells²⁰, we investigated whether either of these two *flhA* mutations might overcome the effects of the loss of both FliJ and FlgN. To clarify this, we introduced these *flhA* alleles into the Δ HIJ B* strain and found that either mutation increased the secretion levels of FlgD and FliC by more than 10 fold (Fig. 4b). Consistently, more than 95% of Δ HIJ B* cells containing either *flhA(D456V)* or *flhA(T490M)* mutation had several flagellar filaments (Fig. 4a, c and Supplementary Table 2) although the average length of those filaments was almost the same as that of the much fewer filaments by the Δ HIJ B* strain (Fig. 4d). The loss of FlgN did not significantly reduce the secretion levels of FlgD and FliC by the Δ HIJ B* cells with either of the *flhA* mutation (Fig. 4b). Furthermore, of the Δ HIJ B* cells containing Δ *flgN::tetRA*, 20.8% with *flhA(D456V)* and 8.5% with *flhA(T490M)* cells produced a single flagellar filament (Fig. 4a) in a way similar to the Δ N mutant strain (Supplementary Fig. 6a). Therefore, we suggest that the *flhA(D456V)* and *flhA(T490M)* mutations can activate the export gate complex to become a highly efficient Na⁺-driven engine in the absence of FliH, FliI, FliJ, and FlgN.

Discussion

The flagellar protein export machinery maintains its activity despite various internal and external perturbations. To do so, this export machinery has evolved to become a dual-fuel export machine to exploit both H⁺ and Na⁺ as the coupling ion¹⁰. The wild-type export engine predominantly uses H⁺ as a coupling ion^{21,23}. However, when the ATPase complex does not work properly, the export engine uses its Na⁺ channel to continue flagellar assembly¹⁰, but the mechanism of the switching of the coupling ion was unknown. Here, we show that an impaired interaction between FliJ and FlhA_C caused by diminished ATPase activity activates Na⁺-coupled protein export (Figs. 1 and 2). We also found that an interaction between FlgN, an export chaperone specific for FlgK and FlgL³³, and FlhA_C becomes essential for Na⁺-coupled protein export (Figs. 3 and 4). FlgN promotes the docking of FlgK and FlgL to the FlhA_C platform of the export gate complex to facilitate rapid and efficient export of these proteins^{35–37}. Therefore, the loss of FlgN reduces the secretion levels of FlgK and FlgL, resulting in a considerable reduction in the probability of filament formation at the tip of the HBB³⁸. We found here that in the $J_{(\Delta 13-24)}$ H* cells, deletion of FlgN inhibits the export of FlgD and FlgE (Fig. 3b). This result suggests that FlgN acts not only as a substrate-specific export chaperone but also as a switch to activate a backup mechanism that in the absence of the FliHIJ ATPase complex, turns on the Na⁺-driven

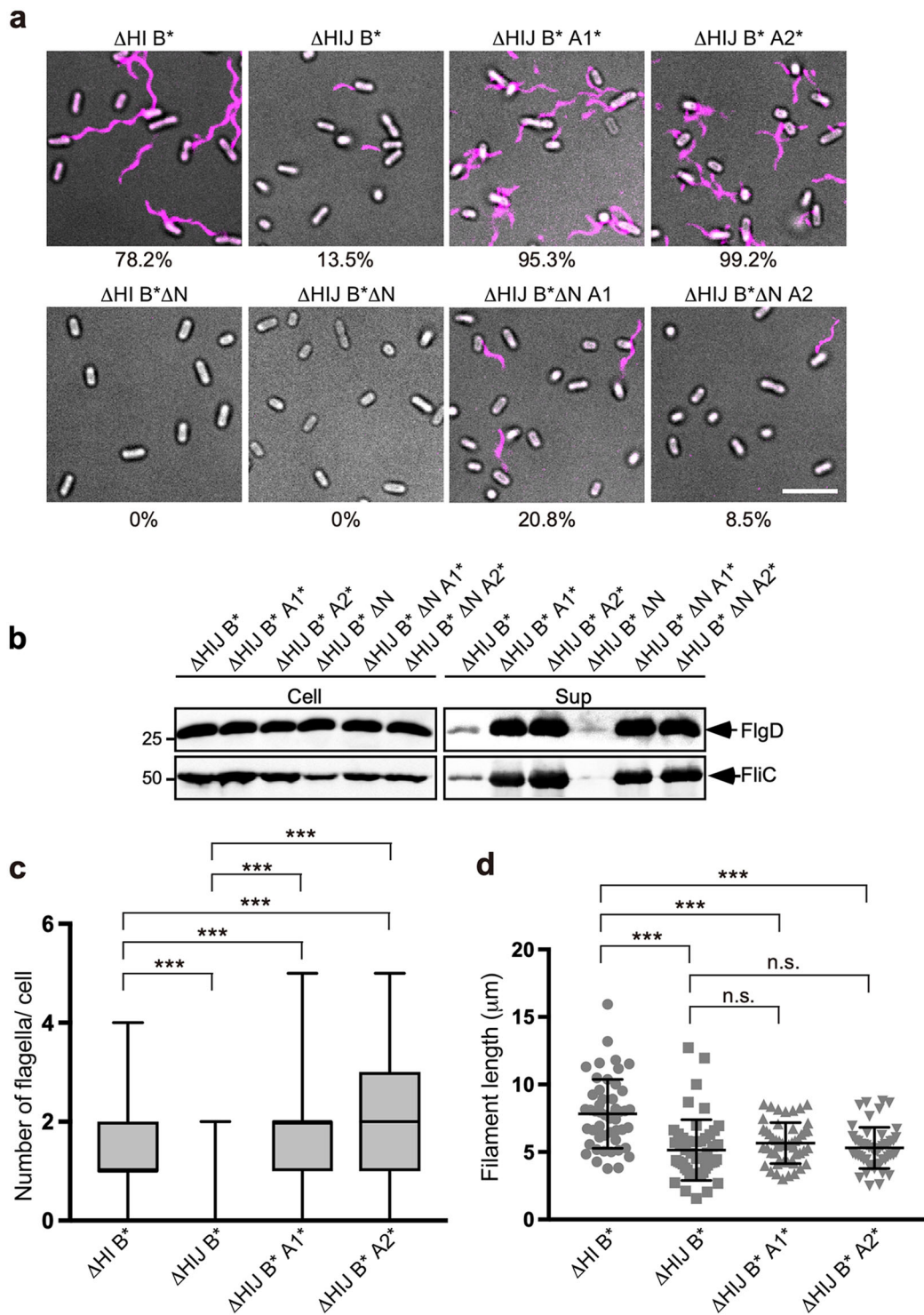


Fig. 4 Effects of gain-of-function mutations in *FlhA* and deletion of *FlgN* on flagellar protein export and assembly by $\Delta HIJ B^*$ cells. **a** Fluorescent images of MMHI0117 ($\Delta HI B^*$), MMHIJ0117 ($\Delta HIJ B^*$), MMHIJ0117-2 ($\Delta HIJ B^* A1^*$), MMHIJ0117-3 ($\Delta HIJ B^* A2^*$), MM9002 ($\Delta HI B^* \Delta N$), MM9004 ($\Delta HIJ B^* \Delta N$), MM9004-2 ($\Delta HIJ B^* \Delta N A1^*$), and MM9004-3 ($\Delta HIJ B^* \Delta N A2^*$). The cells were grown in T-broth (pH 7.5) containing 100 mM NaCl until the cells reached the stationary phase. Flagellar filaments were labelled with Alexa Fluor 594. The fluorescence images of the filaments labelled with Alexa Fluor 594 (magenta) were merged with the bright field images of the cell bodies. Scale bar, 5.0 μm . **b** Immunoblotting, using polyclonal anti-FlgD (1st row) or anti-FlhC (2nd row) antibody, of whole-cell proteins (Cell) and culture supernatant fractions (Sup) prepared from the MMHI0117, MMHIJ0117, MMHIJ0117-2, and MMHIJ0117-3 cells. The regions of interest were cropped from original immunoblots shown in Supplementary Fig. 12. **c, d** Average number and length of flagellar filaments in the MMHI0117, MMHIJ0117, MMHIJ0117-2, and MMHIJ0117-3 cells. Filament length is the average of 50 filaments, and vertical lines are standard deviations. Comparisons between datasets were performed using a two-tailed Student's *t*-test. A *P*-value of <0.05 was considered to be statistically significant difference. ****P* < 0.001; n.s. no statistical significance. (See Supplementary Table 2).

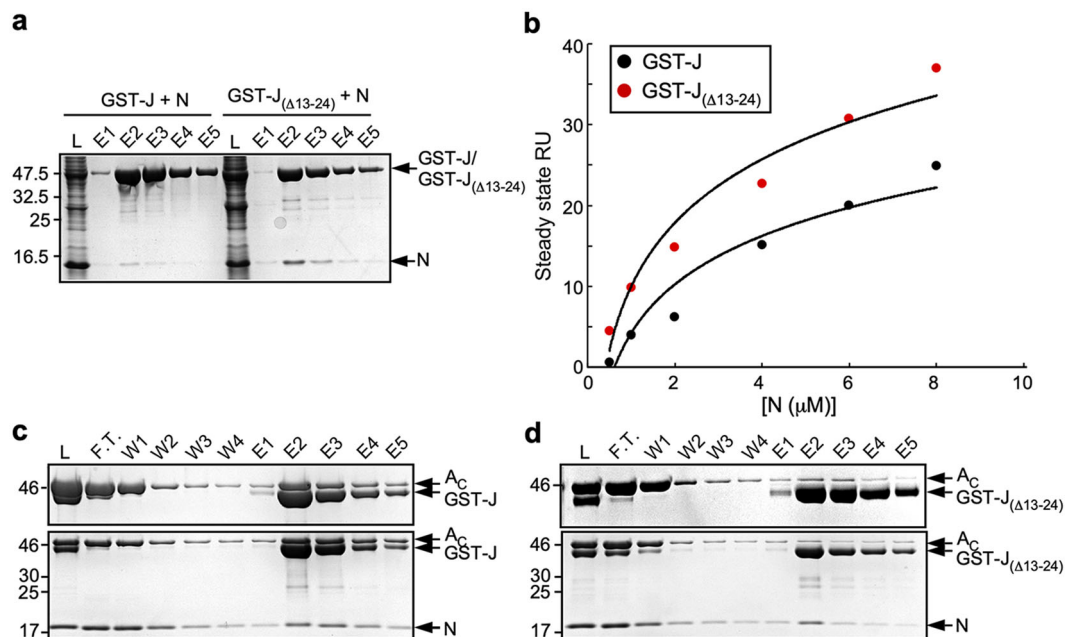


Fig. 5 Effect of a deletion of residues 13–24 of FliJ on interactions of FliJ with FlgN and FlhA_C. **a** Interaction between FliJ and FlgN. Cell lysates prepared from *Salmonella* SJW1368 (Δ *flhDC-cheW*) cells expressing either GST-FliJ (indicated as GST-J) or GST-FliJ(Δ 13–24) (indicated as GST-J(Δ 13–24)) were mixed with those from *E. coli* BL21(DE3) Star cells producing His-FlgN (indicated as N), and then each mixture (indicated as L) was loaded onto a GST column. After extensive washing, proteins were eluted with a buffer containing 10 mM reduced glutathione. Eluted fractions were analyzed by SDS-PAGE with CBB staining. The regions of interest were cropped from original CBB-stained gels shown in Supplementary Fig. 13a. **b** Measurements of the binding affinities of FliJ and FliJ(Δ 13–24) for FlgN by SPR. His-FlgN of various concentrations was flowed over the sensor surface with immobilized GST-FliJ or GST-FliJ(Δ 13–24) in 10 mM HEPES pH 7.4, 0.15 M NaCl, 3 mM EDTA, 0.005% Surfactant P20 at a flow rate of 20 μ l min⁻¹. All experiments were performed at 25 °C. The steady-state resonance units (RU) were plotted against FlgN concentrations. **c, d** Effect of FlgN on the FliJ-FlhA interaction. Purified His-FlhA_C was mixed with purified **c** GST-FliJ or **d** GST-FliJ(Δ 13–24) in the absence (upper panel) and presence (lower panel) of purified His-FlgN, and dialyzed overnight against PBS. Each mixture (L) was loaded onto a GST column. After washing with 10 ml PBS at a flow rate of about 0.5 ml min⁻¹, proteins were eluted with 10 mM reduced glutathione. Flow through fraction (F.T.), wash fractions (W), and elution fractions (E) were analyzed by SDS-PAGE with CBB staining. The regions of interest were cropped from original CBB-stained gels shown in Supplementary Fig. 13b.

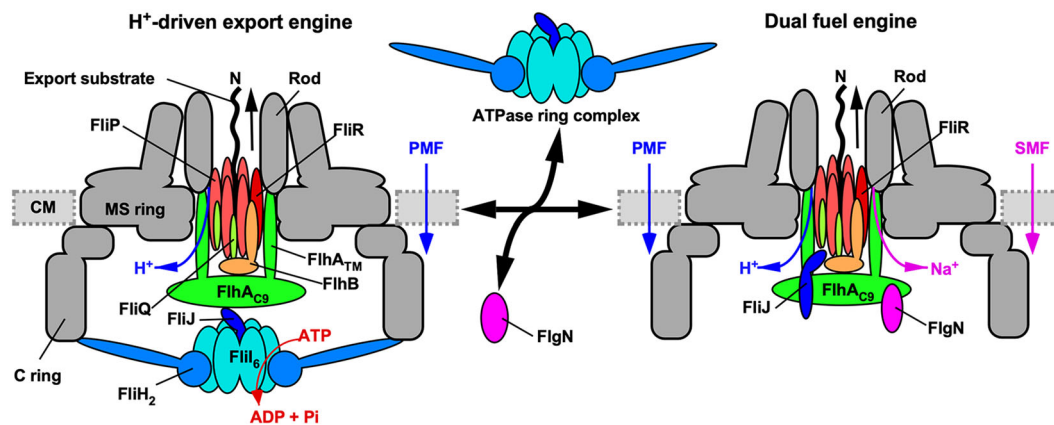


Fig. 6 Schematic diagram of the flagellar protein export machinery. The flagellar protein export machinery is composed of a transmembrane export gate complex made of FlhA, FlhB, FliP, FliQ, and FliR and a cytoplasmic ATPase complex consisting of FliH, FliI, and FliJ. The export gate complex is located inside the MS ring and utilizes proton motive force (PMF) across the cytoplasmic membrane (CM) to drive proton (H⁺)-coupled flagellar protein export. FliP, FliQ and FliR form a polypeptide channel. FlhB associates with the FliP/FliQ/FliR complex and controls opening of the polypeptide channel. The C-terminal cytoplasmic domain of FlhA (FlhA_C) projects into the central cavity of the C ring. The N-terminal transmembrane domain (FlhA_{TM}) forms an ion channel for the translocation of H⁺ and sodium ion (Na⁺) from the periplasm to the cytoplasm. The cytoplasmic ATPase ring complex associates with the C ring through an interaction between FliH and a C ring protein, FliI. ATP hydrolysis by the FliI ATPase activates the export gate complex through an interaction between FliJ and FlhA_C connecting FlhA_C to FlhA_{TM}, becoming an active protein transporter to couple the H⁺ flow through the FlhA channel to the translocation of export substrates into the polypeptide channel. When the cytoplasmic ATPase complex does not function properly, FlgN binds to FlhA_C to open the Na⁺ channel of FlhA_{TM}, allowing the export gate complex to utilize sodium motive force (SMF) across the cytoplasmic membrane to drive Na⁺-coupled protein export.

export engine. FlgN interacts directly and with high affinity with FlhA_C to accomplish this activation (Fig. 6).

The *flhA(D456V)* or *flhA(T490M)* mutation has been isolated as a bypass mutation of the motility defect of the Δ H1 B* Δ N strain³⁵. Here, we found that these *flhA* mutations overcome the effects of loss of both FlgN and FliJ (Fig. 4), suggesting that these two mutations allow FlhA_C to adopt a conformation mimicking its conformation in the active FlgN/FliJ/FlhA_C trimeric complex. Because the interaction between FliJ and FlhA_C is not directly involved in activation of the Na⁺-driven export engine, we propose that the interactions of FlhA_C with FlgN and FliJ activate the Na⁺ channel of FlhA and the polypeptide channel formed by FliP, FliQ, and FliR, respectively, so that the export gate complex efficiently couples the Na⁺ flow through the FlhA channel with substrate entry into the polypeptide channel (Fig. 6).

FlgN binds to a well-conserved hydrophobic dimple of FlhA_C formed by Asp-456, Phe-459, and Thr-490^{35,36,40}. When the ATPase complex is functional, FliJ binds to the flexible linker region of FlhA (FlhA_L) connecting FlhA_C to the N-terminal transmembrane domain that forms an ion channel^{21,41}. This interaction activates the export gate complex to become an active H⁺-driven export engine^{21,42} (Fig. 6). This conclusion is supported by the observation that deletion of residues 328–351 of FlhA_L significantly weakens the FliJ-FlhA_C interaction (Supplementary Fig. 9a) but not the FlgN-FlhA_C interaction (Supplementary Fig. 9b). FlgN bound to FliJ(Δ 13–24) but did not restore the impaired interaction between FliJ(Δ 13–24) and FlhA_C (Fig. 5). FliJ not only binds to FlgN³⁹ but also to the FlgN/FlgK complex³⁵. The FlgN/FlgK/FliJ trimeric complex docks to the FlhA_C platform (Supplementary Fig. 9c)³⁵. When the GST-FlgN/FlgK/FliJ complex was mixed with FlhA_C lacking residues 328–351 of FlhA_L, only a very small amount of FliJ co-purified with this complex (Supplementary Fig. 9c), indicating that FliJ dissociates from FlgN upon binding of the FlgN/FlgK/FliJ complex to FlhA_C lacking residues 328–351 of FlhA_L. Because protein transport activity was higher in the presence of FliJ than in its absence (Fig. 1), we propose that the cytoplasmic FlgN/FliJ complex docks to the FlhA_C platform through an interaction between FlgN and FlhA_C, which then induces the dissociation of the FlgN/FliJ complex into FlgN and FliJ subunits to bind to the hydrophobic dimple of FlhA_C and FlhA_L, respectively. These interactions then fully activate the Na⁺-driven engine of the export gate complex in the absence of an active ATPase complex (Fig. 6). This conclusion is supported by the crystal structure of a FliJ homologue, CdsO, in complex with CdsV_C, which is a FlhA_C homologue⁴³. It remains unknown how FliJ binds to FlhA_L because CdsO does not bind to the linker region of CdsV_C in the crystal structure.

The 3'-5' cyclic diguanylate monophosphate molecule binds to the FliI ATPase to inhibit the FliI ATPase activity²⁴. This event might be expected to inhibit the H⁺-coupled activity of the protein export channel. A subpopulation of planktonic cells is generated during biofilm development, perhaps as a “hedge-betting ploy” for cells to escape the biofilm²⁵. Because the total PMF is quite low in the cells living in the biofilm structure²⁶, we propose that activation of the Na⁺-driven export engine would provide a selective advantage for cells living in the biofilm.

Methods

Bacterial strains, plasmids, transductional crosses, and DNA manipulations.

Wild-type and mutant strains of *S. enterica* serovar Typhimurium and plasmids used in this study are listed in Supplementary Table 3. P22-mediated transductional crosses were carried out with p22HT_{int}. DNA manipulations were performed using standard protocols. DNA sequencing reactions were carried out using BigDye v3.1 (Applied Biosystems) and then the reaction mixtures were analyzed by a 3130 Genetic Analyzer (Applied Biosystems).

Motility assays in soft agar. Fresh colonies were inoculated onto soft agar plates [1% (w/v) tryptone, 10 mM potassium phosphate pH 7.5, 0.35% (w/v) Bacto agar] or soft agar plates containing 100 mM NaCl or 100 mM KCl and incubated at 30 °C. At least ten independent measurements were performed. A diameter of the motility ring of each *Salmonella* strain was measured using ImageJ software version 1.52 (National Institutes of Health).

Secretion assay. Wild-type and mutant cells of *S. enterica* serovar Typhimurium were grown overnight in T-broth [1% (w/v) Bacto tryptone, 10 mM potassium phosphate pH 7.5] without 100 mM NaCl. A 50 μ l of the overnight culture was inoculated into a 5 ml of fresh T-broth (pH 7.5) or T-broth (pH 7.5) containing 100 mM NaCl or 100 mM KCl and incubated at 30 °C with shaking until the cell density had reached an OD₆₀₀ of ca. 1.4–1.6. Cultures were centrifuged to obtain cell pellets and culture supernatants. The cell pellets were resuspended in a sample buffer solution [62.5 mM Tris-HCl, pH 6.8, 2% sodium dodecyl sulfate (SDS), 10% glycerol, 0.001% bromophenol blue] containing 1 μ l of 2-mercaptoethanol. Proteins in the culture supernatants were precipitated by 10% trichloroacetic acid and suspended in a Tris/SDS loading buffer (one volume of 1 M Tris, nine volumes of 1 \times sample buffer solution)⁴⁴ containing 1 μ l of 2-mercaptoethanol. After boiling proteins in both whole cellular and culture supernatant fractions at 95 °C for 3 min, these protein samples were separated by SDS-polyacrylamide gel (normally 12.5% acrylamide) electrophoresis (SDS-PAGE) and transferred to nitrocellulose membranes (Bio-Rad) using a transblotting apparatus (Hoefer). Then, immunoblotting with polyclonal anti-FlgD, anti-FlgE, anti-FlgK, anti-FlgL, or anti-FliC antibody was carried out using iBand Flex Western Device as described in the manufacturer's instructions (Thermo Fisher Scientific). Detection was performed with Amersham ECL Prime western blotting detection reagent (Cytiva). Chemiluminescence signals were captured by a Luminoimage analyzer LAS-3000 (GE Healthcare). All image data were processed with Photoshop software CS6 (Adobe). At least three independent experiments were performed.

Observation of flagellar filaments with a fluorescent dye. Wild-type and mutant cells of *S. enterica* serovar Typhimurium were grown at 30 °C in T-broth (pH 7.5) with or without 100 mM NaCl until the cells reached a stationary phase. The cells were attached to a cover slip (Matsunami glass, Japan), and unattached cells were washed away with motility buffer (10 mM potassium phosphate pH 7.0, 0.1 mM EDTA, 10 mM L-sodium lactate). A 1 μ l aliquot of polyclonal anti-FliC serum was mixed with 50 μ l of motility buffer and then 50 μ l of the mixture was applied to the cells attached to the cover slip. After washing with the motility buffer, 1 μ l of anti-rabbit IgG conjugated with Alexa Fluor 594 (Invitrogen) was added to 50 μ l of motility medium, and then the mixture was applied. After washing with the motility buffer, the cells were observed by fluorescence microscopy⁴⁵. Fluorescence images were analyzed using ImageJ software version 1.52 (National Institutes of Health).

Preparation of HBBs. Wild-type and mutant cells of *S. enterica* serovar Typhimurium were grown at 30 °C in 500 ml of L-broth until the cell density had reached an OD₆₀₀ of ca. 1.0. The cells were harvested by centrifugation (10,000 \times g, 10 min, 4 °C) and suspended in 20 ml of ice-cold 0.1 M Tris-HCl pH 8.0, 0.5 M sucrose, followed by adding EDTA and lysozyme at final concentrations of 10 mM and 0.1 mg ml⁻¹, respectively. The cell suspensions were stirred for 30 min at 4 °C. Then, the cells were solubilized on ice for 1 h by adding Triton X-100 and MgSO₄ at final concentrations of 1% (w/v) and 10 mM, respectively. The cell lysates were adjusted to pH 10.5 with 5 M NaOH and centrifuged (10,000 \times g, 20 min, 4 °C) to remove cell debris. After ultracentrifugation (45,000 \times g, 60 min, 4 °C), pellets were resuspended in 10 mM Tris-HCl, pH 8.0, 5 mM EDTA, 1% (w/v) Triton X-100, and the solution was loaded a 20–50% (w/w) sucrose density gradient in 10 mM Tris-HCl, pH 8.0, 5 mM EDTA, 1% (w/v) Triton X-100. After ultracentrifugation (49,100 \times g, 13 h, 4 °C), intact flagella, HBBs or MS-C rings were collected and ultracentrifuged (60,000 \times g, 60 min, 4 °C). For intact flagella, pellets were resuspended in 50 mM glycine, pH 2.5, 0.1% (w/v) Triton X-100, and were incubated at room temperature for 30 min to depolymerize the filaments. After ultracentrifugation (60,000 \times g, 60 min, 4 °C), pellets were resuspended in 50 μ l of 10 mM Tris-HCl, pH 8.0, 5 mM EDTA, 0.1% (w/v) Triton X-100. Samples were applied to carbon-coated copper grids, followed by negative staining with 2% (w/v) uranyl acetate. Electron micrographs were recorded with a JEM-1011 transmission electron microscope (JEOL, Tokyo, Japan) operated at 100 kV and equipped with a F415 CCD camera (TVIPS, Gauting, Germany) at a magnification of \times 5500, which corresponds to 2.75 nm per pixel.

Pull-down assays by GST chromatography. To identify the flagellar protein required for activation of the Na⁺-driven export engine, GST-FliJ was overproduced in the *Salmonella* MMH10117 strain, and then the cells were suspended in PBS (8 g of NaCl, 0.2 g of KCl, 3.63 g of Na₂HPO₄•12H₂O, 0.24 g of KH₂PO₄, pH 7.4 per liter) and sonicated. After centrifugation of cell lysates to remove undisturbed cells and insoluble membrane fractions, the soluble fractions were loaded onto a glutathione Sepharose 4B column (bed volume, 1 ml) pre-equilibrated with 20 ml of PBS. After extensive washing of the column with PBS, proteins were eluted with 50 mM Tris-HCl, pH 8.0, 10 mM reduced glutathione.

Fractions containing GST or GST-FliJ were identified by SDS-PAGE with Coomassie Brilliant blue (CBB) staining. Then, these fractions were analyzed by immunoblotting with polyclonal anti-FliH_C, anti-FliM, anti-FliN, or anti-FliT antibody.

To analyze the FliN-FliJ interaction by GST affinity chromatography, cell lysates prepared from SJW1368 cells expressing GST-FliJ or GST-FliJ(Δ 13–24), were mixed with those from the *Escherichia coli* BL21 (DE3) Star strain transformed with pMMGN130 (His-FliN). To effect of deletion of residues 328–351 of FliH_L on the interactions of FliH_C with FliN and FliJ, cell lysates prepared from SJW1368 expressing GST-FliN was mixed with purified FliK, purified His-FliJ and the soluble fraction isolated from *E. coli* BL21 (DE3) Star cells over-expressing either His-FliH_C or His-FliH_C lacking residues 328–351 of FliH_L. Then each mixture was loaded onto a Glutathione Sepharose 4B column. After extensive wash of the column with PBS, bound proteins were eluted with 50 mM Tris-HCl, pH 8.0, 10 mM reduced glutathione.

His-FliH_C, His-FliH_{C38K} and His-FliN were overexpressed in *E. coli* BL21 (DE3) Star cells, and then these proteins were purified from the cell lysates by Ni affinity chromatography with a nickel-nitriloacetic acid (Ni-NTA) agarose column (QIAGEN). GST-FliJ, GST-FliJ(Δ 13–24), and GST-FliN were overexpressed in SJW1368 cells, and then these proteins were purified from cell lysates by GST affinity chromatography. To investigate the effect of deletion of residue 13–24 of FliJ on the FliJ-FliH_C interaction, purified His-FliH_C was mixed with purified GST-FliJ or GST-FliJ(Δ 13–24) in the presence and absence of purified His-FliN. To clarify the role of FliH_L on the interactions of FliH_C with FliJ and FliN, purified His-FliH_C or His-FliH_{C38K} was mixed with purified GST-FliJ or GST-FliN. Each mixture was dialyzed overnight against PBS at 4 °C with three changes of PBS. A 5 ml of each mixture was loaded onto a glutathione Sepharose 4B column and washed with 10 ml of PBS at a flow rate of ca. 0.5 ml min⁻¹. Bound proteins were eluted with 5 ml of 50 mM Tris-HCl, pH 8.0, 10 mM reduced glutathione. At least three independent experiments were carried out.

Surface plasmon resonance (SPR). Anti-GST antibody was immobilized on a CM5 chip using a GST capture kit as described in the manufacturer's instructions (GE Healthcare). 40 μ l of 10 μ g ml⁻¹ GST-FliJ or 10 μ g ml⁻¹ of GST-FliJ(Δ 13–24) were injected over the chip pre-equilibrated with a binding buffer (10 mM HEPES pH 7.4, 0.15 M NaCl, 3 mM EDTA, 0.005% Surfactant P20) at a flow rate of 20 μ l min⁻¹ and immobilized on the sensor chip via the anti-GST antibody. Forty microliter of His-FliN of various concentrations in the binding buffer to monitor association was passed over the sensor surface and then washed with the buffer to monitor dissociation at a flow rate of 20 μ l min⁻¹. An acidic buffer (10 mM Glycine-HCl, pH 2.2) was used for regeneration of the surface of the sensor chip by removal of the captured proteins and any associates. All experiments were done at 25 °C. To obtain the K_D value, we analyzed SPR profiles using BIAevaluation software version 4.1 as described in the manufacturer's instructions (GE Healthcare). At least three independent SPR measurements were carried out.

Statistics and reproducibility. Statistical tests, sample size, and number of biological replicates are reported in the figure legends. Statistical analyses were done using Prism 7.0c software (GraphPad). Comparisons were performed using a two-tailed Student's *t*-test. A *P*-value of < 0.05 was considered to be statistically significant difference. **P* < 0.05; ***P* < 0.01; ****P* < 0.001.

Reporting summary. Further information on research design is available in the Nature Research Reporting Summary linked to this article.

Data availability

All data generated during this study are included in this published article and its Supplementary Information files. Strains, plasmids, polyclonal antibodies and all other data are available from the corresponding author on reasonable request.

Received: 27 July 2020; Accepted: 17 February 2021;

Published online: 12 March 2021

References

- Morimoto, Y. V. & Minamino, T. Structure and function of the bi-directional bacterial flagellar motor. *Biomolecules* **4**, 217–234 (2014).
- Nakamura, S. & Minamino, T. Flagella-driven motility of bacteria. *Biomolecules* **9**, 279 (2019).
- Minamino, T. Protein export through the bacterial flagellar type III export pathway. *Biochim. Biophys. Acta* **1843**, 1642–1648 (2014).
- Minamino, T. Hierarchical protein export mechanism of the bacterial flagellar type III protein export apparatus. *FEMS Microbiol. Lett.* **365**, fny117 (2018).
- Galán, J. E., Lara-Tejero, M., Marlovits, T. C. & Wagner, S. Bacterial type III secretion systems: specialized nanomachines for protein delivery into target cells. *Annu. Rev. Microbiol.* **68**, 415–438 (2014).
- Kuhlen, L. et al. Structure of the core of the type III secretion system export apparatus. *Nat. Struct. Mol. Biol.* **25**, 583–590 (2018).
- Ward, E. et al. Type-III secretion pore formed by flagellar protein FliP. *Mol. Microbiol.* **107**, 94–103 (2018).
- Kuhlen, L. et al. The substrate specificity switch FliB assembles onto the export gate to regulate type three secretion. *Nat. Commun.* **11**, 1296 (2020).
- Fukumura, T. et al. Assembly and stoichiometry of the core structure of the bacterial flagellar type III export gate complex. *PLoS Biol.* **15**, e2002281 (2017).
- Minamino, T., Morimoto, Y. V., Hara, N., Aldridge, P. D. & Namba, K. The bacterial flagellar type III export gate complex is a dual fuel engine that can use both H⁺ and Na⁺ for flagellar protein export. *PLoS Pathog.* **12**, e1005495 (2016).
- Erhardt, M. et al. Mechanism of type-III protein secretion: regulation of FliH_A conformation by a functionally critical charged-residue cluster. *Mol. Microbiol.* **104**, 234–249 (2017).
- Minamino, T. & Macnab, R. M. Interactions among components of the *Salmonella* flagellar export apparatus and its substrates. *Mol. Microbiol.* **35**, 1052–1064 (2000).
- Abrusci, P. et al. Architecture of the major component of the type III secretion system export apparatus. *Nat. Struct. Mol. Biol.* **20**, 99–104 (2013).
- Minamino, T., Inoue, Y., Kinoshita, M. & Namba, K. FliK-driven conformational rearrangements of FliH_A and FliB are required for export switching of the flagellar protein export apparatus. *J. Bacteriol.* **202**, e00637–19 (2020).
- Imada, K., Minamino, T., Uchida, Y., Kinoshita, M. & Namba, K. Insight into the flagella type III export revealed by the complex structure of the type III ATPase and its regulator. *Proc. Natl Acad. Sci. USA* **113**, 3633–3638 (2016).
- Minamino, T. & Namba, K. Distinct roles of the FliI ATPase and proton motive force in bacterial flagellar protein export. *Nature* **451**, 485–488 (2008).
- Paul, K., Erhardt, M., Hirano, T., Blair, D. F. & Hughes, K. T. Energy source of flagellar type III secretion. *Nature* **451**, 489–492 (2008).
- Erhardt, M., Mertens, M. E., Fabiani, F. D. & Hughes, K. T. ATPase-independent type-III protein secretion in *Salmonella enterica*. *PLoS Genet.* **10**, e1004800 (2014).
- Minamino, T. et al. FliH and FliI ensure efficient energy coupling of flagellar type III protein export in *Salmonella*. *Microbiologyopen* **5**, 424–435 (2016).
- Inoue, Y., Morimoto, Y. V., Namba, K. & Minamino, T. Novel insights into the mechanism of well-ordered assembly of bacterial flagellar proteins in *Salmonella*. *Sci. Rep.* **8**, 1787 (2018).
- Minamino, T., Morimoto, Y. V., Hara, N. & Namba, K. An energy transduction mechanism used in bacterial type III protein export. *Nat. Commun.* **2**, 475 (2011).
- Minamino, T., Morimoto, Y. V., Kinoshita, M., Aldridge, P. D. & Namba, K. The bacterial flagellar protein export apparatus processively transports flagellar proteins even with extremely infrequent ATP hydrolysis. *Sci. Rep.* **4**, 7579 (2014).
- Morimoto, Y. V. et al. High-resolution pH imaging of living bacterial cell to detect local pH differences. *mBio* **7**, 01911–16 (2016).
- Trampari et al. Bacterial rotary export ATPases are allosterically regulated by the nucleotide second messenger cyclic-di-GMP. *J. Biol. Chem.* **290**, 24470–24483 (2015).
- Houry, A. et al. Bacterial swimmers that infiltrate and take over the biofilm matrix. *Proc. Natl Acad. Sci. USA* **109**, 13088–13093 (2012).
- Prindle, A. et al. Ion channels enable electrical communication in bacterial communities. *Nature* **572**, 59–63 (2015).
- Nakamura, S. et al. Effect of intracellular pH on the torque-speed relationship of bacterial proton-driven flagellar motor. *J. Mol. Biol.* **386**, 332–338 (2009).
- Miesenböck, G., Angelis, D. A. & Rothman, J. E. Visualization secretion and synaptic transmission with pH-sensitive green fluorescent proteins. *Nature* **394**, 192–195 (1998).
- Morimoto, Y. V., Kojima, S., Namba, K. & Minamino, T. M153R mutation in a pH-sensitive green fluorescent protein stabilizes its fusion proteins. *PLoS ONE* **6**, e19598 (2011).
- Hughes, K. T., Gillen, K. L., Semon, M. J. & Karlinsey, J. E. Sensing structural intermediates in bacterial flagellar assembly by export of a negative regulator. *Science* **262**, 1277–1280 (1993).
- Kutsukake, K. Excretion of the anti-sigma factor through a flagellar substructure couples flagellar gene expression with flagellar assembly in *Salmonella typhimurium*. *Mol. Gen. Genet.* **243**, 605–612 (1994).
- Ibuki, T. et al. Interaction between FliJ and FliH_A, components of the bacterial flagellar type III export apparatus. *J. Bacteriol.* **195**, 466–473 (2013).
- Fraser, G. M., Bennett, J. C. Q. & Hughes, C. Substrate-specific binding of hook-associated proteins by FliN and FliT, putative chaperones for flagellum assembly. *Mol. Microbiol.* **32**, 569–580 (1999).

34. Aldridge, P., Karlinsey, J. E. & Hughes, K. T. The type III secretion chaperone FlgN regulates flagellar assembly via a negative feedback loop containing its chaperone substrates FlgK and FlgL. *Mol. Microbiol.* **49**, 1333–1345 (2003).
35. Minamino, T. et al. Interaction of a bacterial flagellar chaperone FlgN with FlhA is required for efficient export of its cognate substrates. *Mol. Microbiol.* **83**, 775–788 (2012).
36. Kinoshita, M., Hara, N., Imada, K., Namba, K. & Minamino, T. Interactions of bacterial chaperone-substrate complexes with FlhA contribute to co-ordinating assembly of the flagellar filament. *Mol. Microbiol.* **90**, 1249–1261 (2013).
37. Kinoshita, M. et al. Rearrangements of α -helical structures of FlgN chaperone control the binding affinity for its cognate substrates during flagellar type III export. *Mol. Microbiol.* **101**, 656–670 (2016).
38. Kutsukake, K., Okada, T., Yokoseki, T. & Iino, T. Sequence analysis of the *flgA* gene and its adjacent region in *Salmonella typhimurium*, and identification of another flagellar gene, *flgN*. *Gene* **143**, 49–54 (1994).
39. Evans, L. D. B., Stafford, G. P., Ahmed, S., Fraser, G. M. & Hughes, C. An escort mechanism for cycling of export chaperones during flagellum assembly. *Proc. Natl Acad. Sci. USA* **103**, 17474–17479 (2006).
40. Inoue, Y. et al. Structural insight into the substrate specificity switch mechanism of the type III protein export apparatus. *Structure* **27**, 965–976 (2019).
41. Bange, G. et al. FlhA provides the adaptor for coordinated delivery of late flagella building blocks to the type III secretion system. *Proc. Natl Acad. Sci. USA* **107**, 11295–11300 (2010).
42. Saijo-Hamano, Y., Minamino, T., Macnab, R. M. & Namba, K. Structural and functional analysis of the C-terminal cytoplasmic domain of FlhA, an integral membrane component of the type III flagellar protein export apparatus in *Salmonella*. *J. Mol. Biol.* **343**, 457–466 (2004).
43. Jensen, J., Yamini, S., Rietsch, A. R. & Spiller, B. W. The structure of the type III secretion system export gate with CdsO, an ATPase lever arm. *PLoS Pathog.* **16**, e1008923 (2020).
44. Minamino, T. & Macnab, R. M. Components of the *Salmonella* flagellar export apparatus and classification of export substrates. *J. Bacteriol.* **181**, 1388–1394 (1999).
45. Morimoto, Y. V., Nakamura, S., Kami-ike, N., Namba, K. & Minamino, T. Charged residues in the cytoplasmic loop of MotA are required for stator assembly into the bacterial flagellar motor. *Mol. Microbiol.* **78**, 1117–1129 (2010).

Acknowledgements

We acknowledge Kelly T. Hughes for his kind gift of the *flgN::tetRA* allele, Kouhei Ohnishi for his kind gift of polyclonal anti-FlgM antibody, Yumi Inoue and Yasuyo Abe

for technical assistance and Michael D. Manson for critical reading of the manuscript and helpful discussions. This work was supported in part by JSPS KAKENHI Grant Numbers JP26293097 and JP19H03182 (to T.M.), JP18K14638 and JP20K15749 (to M.K.), JP15H05593 and JP18K06159 (to Y.V.M.) and JP25000013 (to K.N.) and MEXT KAKENHI Grant Numbers JP15H01640 and JP20H05532 (to T.M.) and JP26115720 and JP15H01335 (to Y.V.M.). This work has also been partially supported by JEOL YOKO-GUSHI Research Alliance Laboratories of Osaka University to K.N.

Author contributions

T.M. and K.N. conceived and designed research; T.M., M.K., and Y.V.M. performed experiments; T.M., M.K., and Y.V.M. analyzed the data, and T.M. and K.N. wrote the paper based on discussion with other authors.

Competing interests

The authors declare no competing interests.

Additional information

Supplementary information The online version contains supplementary material available at <https://doi.org/10.1038/s42003-021-01865-0>.

Correspondence and requests for materials should be addressed to T.M.

Reprints and permission information is available at <http://www.nature.com/reprints>

Publisher's note Springer Nature remains neutral with regard to jurisdictional claims in published maps and institutional affiliations.



Open Access This article is licensed under a Creative Commons Attribution 4.0 International License, which permits use, sharing, adaptation, distribution and reproduction in any medium or format, as long as you give appropriate credit to the original author(s) and the source, provide a link to the Creative Commons license, and indicate if changes were made. The images or other third party material in this article are included in the article's Creative Commons license, unless indicated otherwise in a credit line to the material. If material is not included in the article's Creative Commons license and your intended use is not permitted by statutory regulation or exceeds the permitted use, you will need to obtain permission directly from the copyright holder. To view a copy of this license, visit <http://creativecommons.org/licenses/by/4.0/>.

© The Author(s) 2021